2024 IEEE International Conference on Robotics and Automation (ICRA 2024)
May 13-17, 2024. Yokohama, Japan

Quadratic Programming Based Inverse Kinematics for Precise Bimanual Manipulation

Tomohiro Chaki[1] and Tomohiro Kawakami[1]

***Abstract*— We discuss the precise cooperative motion of a dual manipulator. In the inverse kinematics of cooperative redundant manipulators, a hierarchical method using null space and an optimization method prioritizing the end-effectors relative position in the objective function have been proposed. However, there is no guarantee that the relative position will be maintained in regions subject to joint limits and task-space reachability constraints. As a result, unacceptable errors may occur, and some tasks cannot be accomplished. We propose designing the maximum permissible errors in advance by expressing the target relative position as inequality constraints in the Quadratic Programming (QP) problem. By extending its description to include a virtual spring, we have also achieved subtle force application by two cooperated manipulators. The proposed method was verified by simulation and experiments.**

I. INTRODUCTION

As the development of teleoperated robots [1]–[5] has become more active, the importance of dual-arm manipulation has increased. In the ANA Avatar XPRIZE 2022 [6], remotely controlled mobile manipulators and humanoid robots competed to perform tasks. It is interesting that 18 of the 20 finalist teams were equipped with a dual manipulator despite different mechanical configurations. In addition, an attempt to use the data of the teleoperated dual manipulator for imitation learning has been conducted by [7].

There have been some studies [8] in the past on motion generation for a dual manipulator, and a wide variety of tasks can be performed. In this paper, we focus on bimanual manipulation defined in [9], where each manipulator performs a task toward a common goal while physically interacting with the other. Typical examples of bimanual manipulation include lifting and moving a box and operating a valve with two arms. In such tasks, manipulators must cooperate while maintaining the relative position and orientation of end-effectors (Fig. 1).

To control the relative position and orientation between end-effectors as targeted, the inverse kinematics of each manipulator must continue to have a solution simultaneously. Hence, the manipulators should have redundancy. A well-known method for generating trajectories for a redundant manipulator is the Moore-Penrose pseudo-inverse and its null-space hierarchical method proposed by Khatib [10] and Nakamura [11]. This method allows hierarchically prioritized tasks to be executed as long as the redundancy of the manipulator permits. To apply this method to a bimanual manipulator, a combination with relative Jacobian has been proposed [12], [13]. In this method, the relative position and orientation between the manipulators are expressed through relative Jacobian, and the target position and orientation are set as the first task with the highest priority. However, it should be noted that this method does not explicitly define the error from the target. This is because the solution obtained by the pseudo-inverse matrix is a least-squares one. Therefore, the error may vary in regions subject to joint limits and task-space reachability constraints. Depending on the scene, it may exceed the allowable error, leading to interruption or failure of the task.

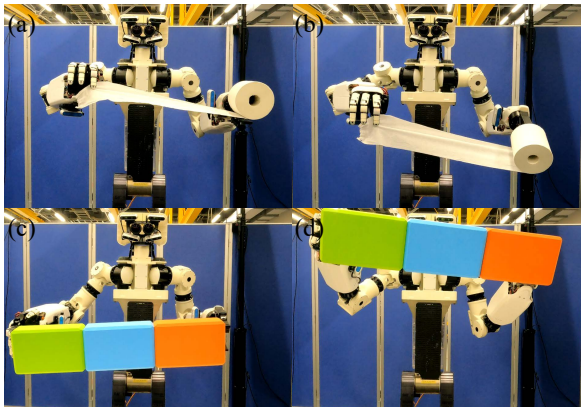

Fig. 1. Experiments of bimanual manipulation. In (a) and (b), two manipulators apply tensile force to toilet paper and keep relative position and orientation without tearing. In (c) and (d), manipulators apply pressing force to three juggling boxes without dropping.

A method of minimizing an objective function consisting of the sum of multiple weighted tasks by QP is also well known. Since this method produces outputs that mediate multiple tasks under equality and inequality constraints, it is frequently used in whole-body motion generation [14]–[16] with a wide range of tasks and constraints. In dual-arm motion generation, Tarbouriech [17] treats the relative position and orientation of the end-effectors as a part of the objective function. However, unexpected errors are still possible because the target relation is formulated as the objective function.

Both methods encounter an issue where it's not possible to establish in advance the maximum error that may occur when trying to achieve the desired relative position and orientation. We propose to introduce the maximum error from the target as inequality constraints of QP. This allows the error to be kept within a predefined constraint while satisfying other

[1] All authors are with Honda R&D Co., Ltd., 8-1 Hon-cho, Wako, Saitama, Japan. {tomohiro_chaki, tomohiro_kawakami}@jp.honda

constraints such as joint limits and self-collision. Since the inequality constraints are expressed in six dimensions in a Cartesian space, the error tolerance can be freely set in each direction. Although inequality constraints are expressed in the dimension of position, inverse kinematics is formulated in the dimension of velocity or acceleration. We obtain an acceleration expression by extending the first-order delay representation of the inequality [18] to the second-order delay. In addition, virtual linkage [19] and virtual impedance admittance [13] have been proposed to apply force to the object. We extend the formulation of inequality constraints to realize a force application by setting virtual springs for each direction.

Section II describes the bimanual constraints we propose. In Section III, we explain the hardware and system overview of our teleoperated robot. Section IV describes how the proposed method is applied to the control system. In Section V, we show the results of bimanual manipulation in both simulation and experiments. Section VI concludes the paper.

II. BIMANUAL CONSTRAINTS IN QP

In this section, we describe how to transform an inequality constraint expression in the position dimension into bimanual constraints in the acceleration dimension.

A. Constraints in QP Based Inverse Kinematics

We solve the QP problem in the dimension of acceleration to maximize hardware performance by considering each joint torque limit that is constrained by actuator performance. A generalized QP is presented below. $\|.\|$ indicates vector squared norm, $\boldsymbol{A}$ and $\boldsymbol{C}$ are the coefficient matrices of $m \times n$ and $p \times n$, respectively, $\boldsymbol{x} \in \boldsymbol{R}^n$, $\boldsymbol{d} \in \boldsymbol{R}^p$, $\boldsymbol{b}^* \in \boldsymbol{R}^m$ is a vector.

$$\min_{\boldsymbol{x}} \quad \|\boldsymbol{A}\boldsymbol{x} - \boldsymbol{b}^*\| \tag{1}$$

$$\text{subject to} \quad \boldsymbol{C}\boldsymbol{x} \leq \boldsymbol{d} \tag{2}$$

Any constraint can be set if it can be expressed in terms of inequality constraints (2). In the following sections, we will describe the process of getting bimanual inequality constraints in the dimension of acceleration.

B. Inequality Constraints on Relative Position and Orientation

Let $\boldsymbol{d} \in \boldsymbol{R}^6$ be the six-dimensional vector of relative position and orientation between end-effectors in task space, $\boldsymbol{d}^*$ be the target, and $\Delta\boldsymbol{d}$ be the maximum allowable error from $\boldsymbol{d}^*$, the inequalities that keep $\boldsymbol{d}$ within the error from the target are as below.

$$\boldsymbol{d}^* - \Delta\boldsymbol{d} \leq \boldsymbol{d} \tag{3}$$

$$\boldsymbol{d} \leq \boldsymbol{d}^* + \Delta\boldsymbol{d} \tag{4}$$

The method of obtaining inequality constraints in the dimension of velocity as the first-order delay expression is known as velocity dumper, and it has been proved that the inequality is satisfied at infinite time [18]. We extend this method to the second-order delay [20], [21] and obtain inequality constraints in the dimension of acceleration without overshooting and oscillation at infinite time by appropriately setting the cutoff angular frequency ω_n and the damping ratio ξ. ω_n should be set to 1/10 or less of the control sampling [22]. The damping ratio ξ is set to ≥ 1 to suppress overshoot and oscillation. As $\boldsymbol{d}_{\text{low}} \triangleq \boldsymbol{d}^* - \Delta\boldsymbol{d}$, $\boldsymbol{d}_{\text{high}} \triangleq \boldsymbol{d}^* + \Delta\boldsymbol{d}$, acceleration expression for (3) and (4) are as below.

$$\omega_n^2(\boldsymbol{d}_{\text{low}} - \boldsymbol{d}) - 2\xi\omega_n\dot{\boldsymbol{d}} \leq \ddot{\boldsymbol{d}} \tag{5}$$

$$\ddot{\boldsymbol{d}} \leq \omega_n^2(\boldsymbol{d}_{\text{high}} - \boldsymbol{d}) - 2\xi\omega_n\dot{\boldsymbol{d}} \tag{6}$$

From this, we have obtained an acceleration expression of the inequality constraints in task space. Starting from the general expression of relative velocity between two objects, we convert (5) and (6) to the form (2).

C. Relative Translational and Rotational Velocity Between Two Objects

In this subsection, starting from the relative velocity between two objects in the world frame $\sum_W$, we obtain their representation in the object frame. Fig. 2 shows the frames $\sum_A$ and $\sum_B$ of Object A and B, respectively, defined to $\sum_W$, and their velocities viewed from each frame. The dashed arrow's starting point indicates the reference frame and the ending point indicates the frame of the object being observed. The position and orientation of Object A and B as seen from $\sum_W$ are $[{}^W\boldsymbol{p}_A, {}^W\boldsymbol{R}_A]$ and $[{}^W\boldsymbol{p}_B, {}^W\boldsymbol{R}_B]$, translational and rotational velocities as $[{}^W\boldsymbol{v}_A, {}^W\boldsymbol{\omega}_A]$ and $[{}^W\boldsymbol{v}_B, {}^W\boldsymbol{\omega}_B]$, the relative velocity of Object B to A in $\sum_W$ is $[{}^W\boldsymbol{v}_{A,B}, {}^W\boldsymbol{\omega}_{A,B}]$. Then, $[{}^W\boldsymbol{v}_B, {}^W\boldsymbol{\omega}_B]$ is expressed by the following equations.

$${}^W\boldsymbol{v}_B = {}^W\boldsymbol{v}_A + {}^W\boldsymbol{v}_{A,B} + {}^W\boldsymbol{\omega}_A \times ({}^W\boldsymbol{p}_B - {}^W\boldsymbol{p}_A) \tag{7}$$

$${}^W\boldsymbol{\omega}_B = {}^W\boldsymbol{\omega}_A + {}^W\boldsymbol{\omega}_{A,B} \tag{8}$$

We define the translational and rotational velocity of Object B to $\sum_A$ as $[{}^A\boldsymbol{v}_B, {}^A\boldsymbol{\omega}_B]$. By using ${}^W\boldsymbol{R}_A$ as a rotation matrix, we obtain the expression ${}^W\boldsymbol{v}_{A,B} = {}^W\boldsymbol{R}_A\, {}^A\boldsymbol{v}_B$ and ${}^W\boldsymbol{\omega}_{A,B} = {}^W\boldsymbol{R}_A\, {}^A\boldsymbol{\omega}_B$. Furthermore, ${}^W\boldsymbol{R}_A$ is an orthogonal matrix, $[{}^A\boldsymbol{v}_B, {}^A\boldsymbol{\omega}_B]$ is obtained by the following equations. ${}^W\boldsymbol{R}_A^T$ indicates transposed matrix of ${}^W\boldsymbol{R}_A$.

$${}^A\boldsymbol{v}_B = {}^W\boldsymbol{R}_A^T\,({}^W\boldsymbol{v}_B - {}^W\boldsymbol{v}_A - {}^W\boldsymbol{\omega}_A \times ({}^W\boldsymbol{p}_B - {}^W\boldsymbol{p}_A)) \tag{9}$$

$${}^A\boldsymbol{\omega}_B = {}^W\boldsymbol{R}_A^T\,({}^W\boldsymbol{\omega}_B - {}^W\boldsymbol{\omega}_A) \tag{10}$$

From this, the relative translational and rotational velocities of Object A and B to $\sum_A$ could be obtained. However, the discussion is still limited in the dimension of velocity, we will explain the process of deriving an expression for joint angular acceleration that can be applied to QP.

D. Joint Angular Acceleration Expression of Relative Translational and Rotational Acceleration

We redefine $[{}^W\boldsymbol{p}_A, {}^W\boldsymbol{R}_A]$, $[{}^W\boldsymbol{v}_A, {}^W\boldsymbol{\omega}_A]$, $[{}^W\boldsymbol{p}_B, {}^W\boldsymbol{R}_B]$ and $[{}^W\boldsymbol{v}_B, {}^W\boldsymbol{\omega}_B]$ in the previous subsection as the end-effector position and velocity of the manipulator A and B, respectively. The Jacobians of each manipulator are $\boldsymbol{J}_A$ and

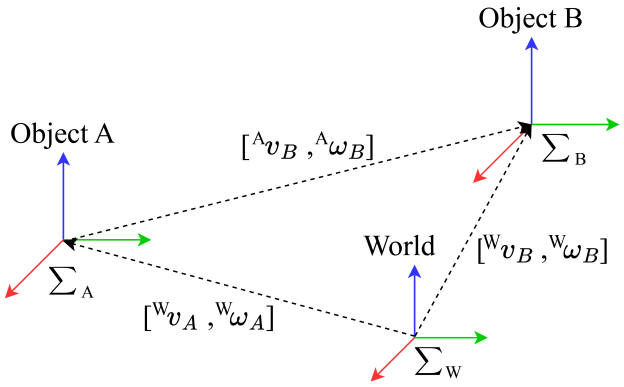

Fig. 2. Relative velocity between two objects

$\boldsymbol{J}_B$, and the joint angular velocity vectors $\dot{\boldsymbol{q}}_A$ and $\dot{\boldsymbol{q}}_B$ are summarized as $\dot{\boldsymbol{q}} = [\dot{\boldsymbol{q}}_A^T, \dot{\boldsymbol{q}}_B^T]^T \in \boldsymbol{R}^{2n}$. Equation (9) and (10) can be organized into the following matrix representation.

$$\begin{bmatrix} {}^{A}\boldsymbol{v}_B \\ {}^{A}\boldsymbol{\omega}_B \end{bmatrix} = \begin{bmatrix} {}^{W}\boldsymbol{R}_A^T & \boldsymbol{0} \\ \boldsymbol{0} & {}^{W}\boldsymbol{R}_A^T \end{bmatrix} \left[\begin{bmatrix} -\boldsymbol{J}_A & \boldsymbol{J}_B \end{bmatrix} \dot{\boldsymbol{q}} - \begin{bmatrix} {}^{W}\boldsymbol{\omega}_A \times ({}^{W}\boldsymbol{p}_B - {}^{W}\boldsymbol{p}_A) \\ \boldsymbol{0} \end{bmatrix} \right] \tag{11}$$

We focus on the second term of the equation $({}^{W}\boldsymbol{R}_A^T\, {}^{W}\boldsymbol{\omega}_A \times ({}^{W}\boldsymbol{p}_B - {}^{W}\boldsymbol{p}_A))$. The three unit vectors that make up the rotation matrix ${}^{W}\boldsymbol{R}_A$ are ${}^{W}_{0}\boldsymbol{r}_A$, ${}^{W}_{1}\boldsymbol{r}_A$, ${}^{W}_{2}\boldsymbol{r}_A$, hence its transpose matrix ${}^{W}\boldsymbol{R}_A^T$ is as below.

$${}^{W}\boldsymbol{R}_A^T = \begin{bmatrix} {}^{W}_{0}\boldsymbol{r}_A^T \\ {}^{W}_{1}\boldsymbol{r}_A^T \\ {}^{W}_{2}\boldsymbol{r}_A^T \end{bmatrix} \tag{12}$$

From this, ${}^{W}\boldsymbol{R}_A^T\, {}^{W}\boldsymbol{\omega}_A \times ({}^{W}\boldsymbol{p}_B - {}^{W}\boldsymbol{p}_A)$ is expressed as a scalar triple product consisting of the dot and cross products of the vectors.

$${}^{W}\boldsymbol{R}_A^T\, {}^{W}\boldsymbol{\omega}_A \times ({}^{W}\boldsymbol{p}_B - {}^{W}\boldsymbol{p}_A) = \begin{bmatrix} {}^{W}_{0}\boldsymbol{r}_A \cdot ({}^{W}\boldsymbol{\omega}_A \times ({}^{W}\boldsymbol{p}_B - {}^{W}\boldsymbol{p}_A)) \\ {}^{W}_{1}\boldsymbol{r}_A \cdot ({}^{W}\boldsymbol{\omega}_A \times ({}^{W}\boldsymbol{p}_B - {}^{W}\boldsymbol{p}_A)) \\ {}^{W}_{2}\boldsymbol{r}_A \cdot ({}^{W}\boldsymbol{\omega}_A \times ({}^{W}\boldsymbol{p}_B - {}^{W}\boldsymbol{p}_A)) \end{bmatrix} \tag{13}$$

Let ${}^{\omega}\boldsymbol{J}_A$ be the Jacobian of $3 \times n$, which is the element related to manipulator rotational velocity extracted from $\boldsymbol{J}_A$. By utilizing the circularity of the scalar triple product, the joint angular velocity $\dot{\boldsymbol{q}}_A$ is extracted from (13).

$${}^{W}\boldsymbol{R}_A^T\, {}^{W}\boldsymbol{\omega}_A \times ({}^{W}\boldsymbol{p}_B - {}^{W}\boldsymbol{p}_A) = \begin{bmatrix} (({}^{W}\boldsymbol{p}_B - {}^{W}\boldsymbol{p}_A) \times {}^{W}_{0}\boldsymbol{r}_A)^T \\ (({}^{W}\boldsymbol{p}_B - {}^{W}\boldsymbol{p}_A) \times {}^{W}_{1}\boldsymbol{r}_A)^T \\ (({}^{W}\boldsymbol{p}_B - {}^{W}\boldsymbol{p}_A) \times {}^{W}_{2}\boldsymbol{r}_A)^T \end{bmatrix} {}^{\omega}\boldsymbol{J}_A \dot{\boldsymbol{q}}_A \tag{14}$$

We also define the Jacobian ${}^{\omega}\boldsymbol{J}_{A,0}$ of size $3 \times 2n$ reconstructed from ${}^{\omega}\boldsymbol{J}_A$ and the zero matrix as below.

$${}^{\omega}\boldsymbol{J}_{A,0} \triangleq \begin{bmatrix} {}^{\omega}\boldsymbol{J}_A & \boldsymbol{0} \end{bmatrix} \tag{15}$$

From (14) and (15), the end-effectors relative velocity (11) becomes as follows.

$$\begin{aligned} \begin{bmatrix} {}^{A}\boldsymbol{v}_B \\ {}^{A}\boldsymbol{\omega}_B \end{bmatrix} &= \begin{bmatrix} {}^{W}\boldsymbol{R}_A^T & \boldsymbol{0} \\ \boldsymbol{0} & {}^{W}\boldsymbol{R}_A^T \end{bmatrix} \begin{bmatrix} -\boldsymbol{J}_A & \boldsymbol{J}_B \end{bmatrix} \dot{\boldsymbol{q}} \\ &\quad - \begin{bmatrix} (({}^{W}\boldsymbol{p}_B - {}^{W}\boldsymbol{p}_A) \times {}^{W}_{0}\boldsymbol{r}_A)^T \\ (({}^{W}\boldsymbol{p}_B - {}^{W}\boldsymbol{p}_A) \times {}^{W}_{1}\boldsymbol{r}_A)^T \\ (({}^{W}\boldsymbol{p}_B - {}^{W}\boldsymbol{p}_A) \times {}^{W}_{2}\boldsymbol{r}_A)^T \\ \boldsymbol{0} \end{bmatrix} {}^{\omega}\boldsymbol{J}_{A,0}\dot{\boldsymbol{q}} \end{aligned} \tag{16}$$

We define the coefficient matrices $\boldsymbol{X}$ and $\boldsymbol{Y}$.

$$\boldsymbol{X} \triangleq \begin{bmatrix} {}^{W}\boldsymbol{R}_A^T & \boldsymbol{0} \\ \boldsymbol{0} & {}^{W}\boldsymbol{R}_A^T \end{bmatrix} \begin{bmatrix} -\boldsymbol{J}_A & \boldsymbol{J}_B \end{bmatrix} \tag{17}$$

$$\boldsymbol{Y} \triangleq \begin{bmatrix} (({}^{W}\boldsymbol{p}_B - {}^{W}\boldsymbol{p}_A) \times {}^{W}_{0}\boldsymbol{r}_A)^T \\ (({}^{W}\boldsymbol{p}_B - {}^{W}\boldsymbol{p}_A) \times {}^{W}_{1}\boldsymbol{r}_A)^T \\ (({}^{W}\boldsymbol{p}_B - {}^{W}\boldsymbol{p}_A) \times {}^{W}_{2}\boldsymbol{r}_A)^T \\ \boldsymbol{0} \end{bmatrix} {}^{\omega}\boldsymbol{J}_{A,0} \tag{18}$$

From the above, the end-effector translational and rotational velocity of manipulator B to manipulator A $[{}^{A}\boldsymbol{v}_B, {}^{A}\boldsymbol{\omega}_B]$, and its acceleration $[{}^{A}\boldsymbol{a}_B, {}^{A}\boldsymbol{\alpha}_B]$ are as follows.

$$\begin{bmatrix} {}^{A}\boldsymbol{v}_B \\ {}^{A}\boldsymbol{\omega}_B \end{bmatrix} = (\boldsymbol{X} - \boldsymbol{Y})\dot{\boldsymbol{q}} \tag{19}$$

$$\begin{bmatrix} {}^{A}\boldsymbol{a}_B \\ {}^{A}\boldsymbol{\alpha}_B \end{bmatrix} = (\boldsymbol{X} - \boldsymbol{Y})\ddot{\boldsymbol{q}} + (\dot{\boldsymbol{X}} - \dot{\boldsymbol{Y}})\dot{\boldsymbol{q}} \tag{20}$$

Finally, the relative translational and rotational accelerations can be expressed using the joint angular acceleration $\ddot{\boldsymbol{q}}$.

E. Bimanual Inequality Constraints on Relative Position and Orientation

We convert (20) to the inequality constraint representation of (2). Using the fact that $\ddot{\boldsymbol{d}}$ is expressed in terms of joint angular acceleration $\ddot{\boldsymbol{q}}$ and velocity $\dot{\boldsymbol{q}}$ in (20), we obtain the following inequality constraints for the terms related to $\ddot{\boldsymbol{q}}$.

$$\omega_n^2(\boldsymbol{d}_{\text{low}} - \boldsymbol{d}) - 2\xi\omega_n\dot{\boldsymbol{d}} - (\dot{\boldsymbol{X}} - \dot{\boldsymbol{Y}})\dot{\boldsymbol{q}} \leq (\boldsymbol{X} - \boldsymbol{Y})\ddot{\boldsymbol{q}} \tag{21}$$

$$(\boldsymbol{X} - \boldsymbol{Y})\ddot{\boldsymbol{q}} \leq \omega_n^2(\boldsymbol{d}_{\text{high}} - \boldsymbol{d}) - 2\xi\omega_n\dot{\boldsymbol{d}} - (\dot{\boldsymbol{X}} - \dot{\boldsymbol{Y}})\dot{\boldsymbol{q}} \tag{22}$$

Starting from inequality constraints on the relative position and orientation (3), (4), we finally get bimanual constraints (21) and (22) in QP. Practically, the derivative variables in the equations are obtained by numerical differentiation.

F. Applying Force by Adding A Virtual Spring Characteristic

In actual bimanual manipulations, since the work is often performed by applying force to the object, it is desirable to be able to generate force between the end-effectors in addition to maintaining relative position. Then, for $\boldsymbol{d}^*$ introduced in (3) and (4), we define a new $\boldsymbol{d}^*_{\text{spring}}$ by adding a virtual spring term to $\boldsymbol{d}^*$. Note that $\oslash$ is an element-wise division of the matrix (Hadamard division).

$$\boldsymbol{d}^*_{\text{spring}} \triangleq \boldsymbol{d}^* + \boldsymbol{f} \oslash \boldsymbol{k} \tag{23}$$

By setting the spring constant $\boldsymbol{k}$ according to the object and the contact force $\boldsymbol{f}$ arbitrarily, it is possible to apply force to the object. We set $\boldsymbol{d}_{\text{low}}$ and $\boldsymbol{d}_{\text{high}}$ to the following (24)

and (25), respectively. Again, since $\boldsymbol{f}$ is a six-dimensional vector, it can generate force independently in each direction of position and orientation.

$$\boldsymbol{d}_{\text{low}} = \boldsymbol{d}^{*}_{\text{spring}} - \Delta\boldsymbol{d} \tag{24}$$

$$\boldsymbol{d}_{\text{high}} = \boldsymbol{d}^{*}_{\text{spring}} + \Delta\boldsymbol{d} \tag{25}$$

III. Overview of the Avatar Robot

In this section, we describe the overview of the avatar robot on both the Hardware and Software side.

A. Hardware

Our avatar robot is based on the torque-controlled humanoid robot E2DR [23], [24]. The avatar robot has a hardware configuration suitable for verification in general work environments with differential two wheels and end-effectors. It is a dual-armed robot with a right arm equipped with an eight-degrees-of-freedom (DoF) redundant manipulator and an 11-DoF wire-driven multi-fingered hand that is a smaller and lighter version of [25], and a left arm equipped with a same manipulator and a general two-fingered gripper. The robot is composed of 34-DoF in total, including one DoF for tilting the head equipped with an RGB camera, three for the torso, one for the gripper, and two differential wheels. The manipulator is composed of eight-DoF, with the two-DoF located at the tip being driven by wires due to the integrated structure of the multi-fingered hand. The remaining six are driven directly by the actuator via a reduction gear.

B. Software

An overview of our teleoperation system is shown in Fig. 3. The first component, Desired End-Effector Pose Generator (Fig. 3(a)) gets the end-effectors commands generated by a commercially available motion capture device that acquires the position and orientation of the operator's wrist in task space or by GUI inputs. It performs coordinate transformation and filtering and outputs the resulting dual-armed end-effector command $\boldsymbol{x}_{\text{des}} \in \boldsymbol{R}^{6\times 2}$. By solving the QP problem in Acceleration-Based Inverse Kinematics (Fig. 3(b)), we obtain the joint angular acceleration command $\ddot{\boldsymbol{q}}_{\text{ref}} \in \boldsymbol{R}^{2n}$. The formulation of QP is described in detail in Section IV. Next, the joint space commands obtained from Fig. 3(b) are input to the Torque-Based Stabilizer (Fig. 3(c)) that receives sensor feedback $\dot{\boldsymbol{q}}_{\text{state}}$ and $\boldsymbol{q}_{\text{state}}$ from the robot and generates the final joint torque command $\boldsymbol{\tau}_{\text{out}} \in \boldsymbol{R}^{2n}$. The bimanual constraints proposed in this paper can be implemented using the QP in Fig. 3(b), and it does not matter the type of stabilizer and lower controller.

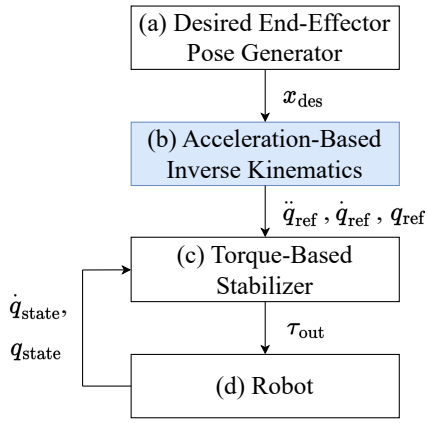

Fig. 3. Overall structure of teleoperation control system

IV. Whole-Body QP formulation

This section describes how to apply bimanual constraints (21) and (22) to the whole-body QP formulation in the Acceleration-Based Inverse Kinematics (Fig. 3(b)).

A. Objective Function

In (1), we construct the objective function with the following two tasks.

- End-effectors acceleration task
- Joint angular acceleration task

The target $\ddot{\boldsymbol{x}}_{\text{cmd}} \in \boldsymbol{R}^{6\times 2}$ for the end-effectors acceleration task is calculated by a Proportional-Derivative (PD) control law based on the target end-effectors position and orientation $\boldsymbol{x}_{\text{des}}$. $\boldsymbol{x}_{\text{ref, pre}}$ and $\dot{\boldsymbol{x}}_{\text{ref, pre}}$ are derived from the previous outputs of Acceleration-Based Inverse Kinematics respectively. K and D are gains for the PD controller.

$$\ddot{\boldsymbol{x}}_{\text{cmd}} = K(\boldsymbol{x}_{\text{des}} - \boldsymbol{x}_{\text{ref, pre}}) + D(\dot{\boldsymbol{x}}_{\text{des}} - \dot{\boldsymbol{x}}_{\text{ref, pre}}) \tag{26}$$

This is the method to generate $\ddot{\boldsymbol{x}}_{\text{cmd}}$ in the normal case, but during performing a bimanual task, the following constraint is applied so that the homogeneous transformation matrix $\boldsymbol{T}$ between $\boldsymbol{x}_{\text{des, primary}}$ and $\boldsymbol{x}_{\text{des, secondary}}$ is constant.

$$\boldsymbol{x}_{\text{des, secondary}} = \boldsymbol{T}\boldsymbol{x}_{\text{des, primary}} \tag{27}$$

We define $\boldsymbol{x}_{\text{des, bi}} \triangleq [\boldsymbol{x}^{T}_{\text{des, primary}}, \boldsymbol{x}^{T}_{\text{des, secondary}}]^{T}$.

$$\begin{aligned}\ddot{\boldsymbol{x}}_{\text{cmd, bi}} = K(\boldsymbol{x}_{\text{des, bi}} - \boldsymbol{x}_{\text{ref, pre}}) \\ + D(\dot{\boldsymbol{x}}_{\text{des, bi}} - \dot{\boldsymbol{x}}_{\text{ref, pre}})\end{aligned} \tag{28}$$

Assuming the Jacobian of a dual manipulator to be $\boldsymbol{J}$ and the joint angle to be $\boldsymbol{q}$, the objective function of the end-effectors acceleration task is defined as follows.

$$\|\boldsymbol{J}\ddot{\boldsymbol{q}} - \ddot{\boldsymbol{x}}_{\text{cmd, bi}} + \dot{\boldsymbol{J}}\dot{\boldsymbol{q}}\| \tag{29}$$

The joint angular acceleration task is introduced to suppress steep and discontinuous motions. In order to minimize the difference between the previous command value of joint angular acceleration $\ddot{\boldsymbol{q}}_{\text{ref, pre}}$, the objective function is set as follows.

$$\|\ddot{\boldsymbol{q}} - \ddot{\boldsymbol{q}}_{\text{ref, pre}}\| \tag{30}$$

As a weighted sum of these two tasks, the objective function of the QP problem is as follows. Let W_1 and W_2 be the weights of each task.

$$\|\boldsymbol{J}\ddot{\boldsymbol{q}} - \ddot{\boldsymbol{x}}_{\text{cmd, bi}} + \dot{\boldsymbol{J}}\dot{\boldsymbol{q}}\|_{W_1} + \|\ddot{\boldsymbol{q}} - \ddot{\boldsymbol{q}}_{\text{ref, pre}}\|_{W_2} \tag{31}$$

B. Inequality Constraints

The inequality constraints consist of the following three, including the bimanual constraints (21) and (22).

- Joint angular acceleration constraints
- Joint actuator T-N constraints
- Bimanual constraints

The lower and upper joint angle limits are $\boldsymbol{q}_{\text{low}}$ and $\boldsymbol{q}_{\text{high}}$, respectively. Joint angular acceleration constraints can be expressed as well as (5) and (6).

$$\omega_n^2(\boldsymbol{q}_{\text{low}} - \boldsymbol{q}) - 2\xi\omega_n\dot{\boldsymbol{q}} \leq \ddot{\boldsymbol{q}} \tag{32}$$

$$\ddot{\boldsymbol{q}} \leq \omega_n^2(\boldsymbol{q}_{\text{high}} - \boldsymbol{q}) - 2\xi\omega_n\dot{\boldsymbol{q}} \tag{33}$$

Joint actuator T-N constraints are introduced for hardware protection and bringing out the actuator potential. Let $\boldsymbol{\tau}_{\text{low}}(\dot{\boldsymbol{q}})$, $\boldsymbol{\tau}_{\text{high}}(\dot{\boldsymbol{q}})$ be the lower and upper limits of torque determined from the specifications of each joint actuator and reduction gear, and $\boldsymbol{I}$ be the inertia matrix. The following inequality constraints are obtained.

$$\boldsymbol{\tau}_{\text{low}}(\dot{\boldsymbol{q}}) \leq \boldsymbol{I}\ddot{\boldsymbol{q}} \tag{34}$$

$$\boldsymbol{I}\ddot{\boldsymbol{q}} \leq \boldsymbol{\tau}_{\text{hign}}(\dot{\boldsymbol{q}}) \tag{35}$$

Including bimanual constraints (21) and (22), three inequality constraints for each lower/upper limit are set. Then, we obtain the joint angular acceleration command $\ddot{\boldsymbol{q}}$ by solving the QP problem to minimize (31) under constraints. The joint angular velocity command $\dot{\boldsymbol{q}}$ and the joint angle command $\boldsymbol{q}$ are obtained by the first-order and second-order integration, respectively.

V. EXPERIMENTAL RESULTS

This section presents the results and discussion of applying the bimanual constraints to the actual robot system. The following two experiments were conducted to verify the proposed method.

- Verification of relative position and orientation maintenance between the end-effectors on a predefined trajectory
- Applying force to example objects by a virtual spring

A. Verification of Relative Position and Orientation Maintenance

First, to confirm the basic effect of the bimanual constraints, we input a predefined sine wave trajectory (TABLE I) to Acceleration-Based Inverse Kinematics (Fig. 3(b)). We verify whether the relative position and orientation are within the maximum permissible error $\Delta\boldsymbol{d}$ in (3) and (4). Parameters in the inequalities (3), (4), (21) and (22) are set to the values in TABLE II. Let $\Delta\boldsymbol{d}_p = [\Delta d_p, \Delta d_p, \Delta d_p]^T$ and $\Delta\boldsymbol{d}_o = [\Delta d_o, \Delta d_o, \Delta d_o]^T$ be the permissible errors of position and orientation, respectively. Note that even if the bimanual constraints (21) and (22) are not introduced, the end-effectors acceleration task (29) will maintain relative position and orientation to the extent possible. Hereafter, in the description of the resulting plots (Fig. 5), the sine wave trajectory is referred to as "reference" (dotted line), the case where the relative position and orientation maintained by the end-effectors acceleration task as "task" (dashed line), and the case where the bimanual constraints introduced as "constrained" (solid line). The transition of the robot model on the visualization tool RViz [26] shown in Fig. 4 corresponds to the time on the horizontal axis in Fig. 5. The purple markers are the end-effectors commands, indicating that a wide range of commands are input, even those that exceed the manipulator's reachability. Fig. 5(a) shows the transition of the right end-effector position, and (c) shows the error from the target relative position $\boldsymbol{d}^*$. The horizontal solid lines drawn constant at ± 0.015 [m] mean the tolerance Δd_p. We can see that "task" moves beyond Δd_p as "reference" goes far from the robot, while "constrained" continues to stay between $\pm\Delta d_p$. Fig. 5(b) shows the transition of the right end-effector orientation and (d) shows the orientation error from $\boldsymbol{d}^*$. The "constrained" stays within $\pm\Delta d_o$ (± 2 [deg]) most of the time, but around 13 [sec], "ψ-constrained" temporarily exceeds $-\Delta d_o$ and then quickly returns within tolerance. It is considered to be the effect of sampling in discrete time because the joint angular acceleration $\ddot{\boldsymbol{q}}$ calculated by the QP at sampling time t is constant until a new solution is obtained at the next step $t + \Delta t$. This effect may be reduced by increasing the sampling frequency or by predicting the joint angular acceleration state until the next time step.

B. Applying Force to Example Objects by A Virtual Spring

The lower and upper limits of the relative position and orientation between the end-effectors are set to (24) and (25) including a virtual spring, respectively, and we use the actual robot to apply force to example objects. To verify the effect of the coordinated force application by the dual-armed manipulator, we selected toilet paper that tears easily and juggling boxes that easily fall when the force balance is lost. Fig. 1(a) and (b) show that the manipulators apply a tensile force to toilet paper. Since the force is based on the relative position and orientation of the end-effectors, it can be seen that the manipulators maintain the object's shape and

TABLE I
INPUT SINE WAVE PARAMETERS

Position Amplitude [m]	Orientation Amplitude [deg]	Frequency [Hz]	Phase
0.35	10	0.01	0-$\pi/4$

TABLE II
INEQUALITY CONSTRAINTS PARAMETERS

$\boldsymbol{\omega}_n$ [rad/s]	ξ	Δd_p [m]	Δd_o [deg]
20	1	0.015	2

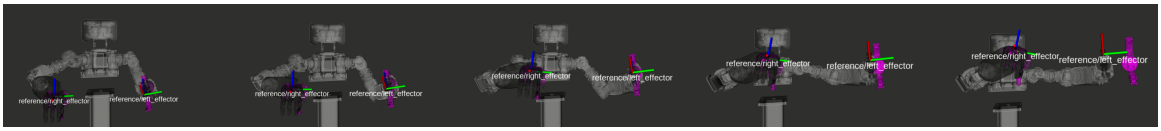

Fig. 4. Snapshots of a predefined trajectory motion

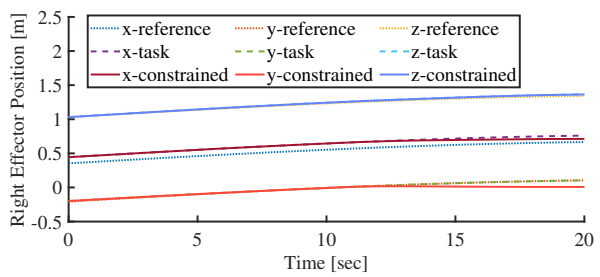

(a) Right end-effector transition of position

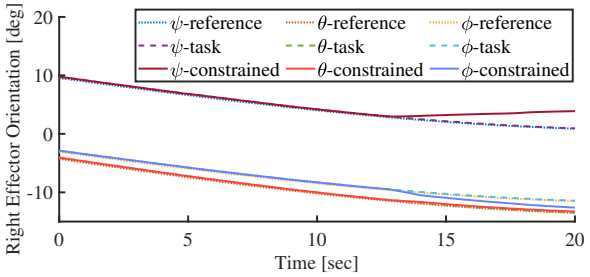

(b) Right end-effector transition of orientation

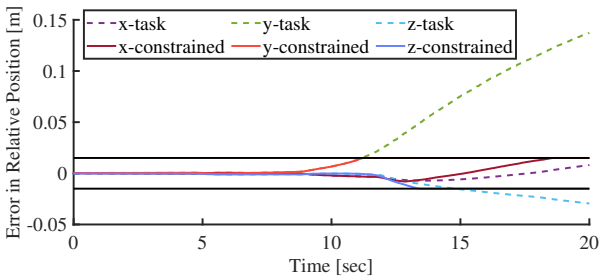

(c) Relative position error between the end-effectors

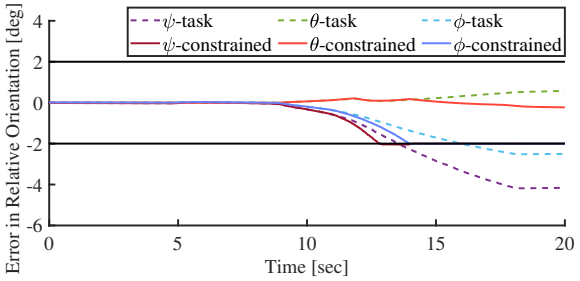

(d) Relative orientation error between the end-effectors

Fig. 5. Right end-effector trajectory and relative error between the end-effectors. "constrained" errors are strictly suppressed in ± 0.015 [m] for position and ± 2 [deg] for orientation.

apply a tension force to the paper's edges simultaneously. Fig. 1(c) and (d) show how a pushing force is applied to three boxes. This is a scene in which the object could be grasped stably, but the object would immediately fall if the relative position and orientation between the end-effectors were not maintained. In the case of an object falling due to slippage at the contact points, the risk of interference between the two manipulators or collision with surrounding objects can be suppressed because the method is based on position control. These results confirm the effectiveness of the proposed method for a force application by a dual-armed manipulator that does not require force sensors on each end-effector.

VI. CONCLUSIONS

- We have proposed the inverse kinematics method for bimanual manipulation that allows the design of the maximum permissible errors in relative position and orientation between the end-effectors in advance. The method allows the errors to be kept within the constraints by expressing the target relative position and orientation as inequality constraints of the QP problem.
- By extending the description of inequality constraints to include a virtual spring, the method realizes a force application by a cooperative dual-armed manipulator without force sensors.
- This method can be applied to cooperative actions with three or more manipulators by defining inequality constraints according to the target robot configurations. It is also expected to be introduced as a supporting function for a teleoperated robot to realize smooth operation.

REFERENCES

[1] K. Darvish, L. Penco, J. Ramos, R. Cisneros, J. Pratt, E. Yoshida, S. Ivaldi, and D. Pucci, "Teleoperation of humanoid robots: A survey," *IEEE Transactions on Robotics*, vol. 39, no. 3, pp. 1706–1727, 2023.

[2] "Honda Takes on Challenges to Create Avatar Robots Applying ASIMO Technologies to the Next Generation Robots — Honda Stories," 2022. [Online]. Available: https://global.honda/stories/025/

[3] "Teleoperation System," 2023. [Online]. Available: https://www.shadowrobot.com/teleoperation/

[4] "SANCTUARY AI," 2023. [Online]. Available: https://sanctuary.ai/

[5] L. Penco, N. Scianca, V. Modugno, L. Lanari, G. Oriolo, and S. Ivaldi, "A multimode teleoperation framework for humanoid loco-manipulation: An application for the icub robot," *IEEE Robotics Automation Magazine*, vol. 26, no. 4, pp. 73–82, 2019.

[6] "ANA Avatar XPRIZE," 2022. [Online]. Available: https://avatar.xprize.org/prizes/avatar

[7] T. Z. Zhao, V. Kumar, S. Levine, and C. Finn, "Learning fine-grained bimanual manipulation with low-cost hardware," in *Robotics: Science and Systems XIX, Daegu, Republic of Korea, July 10-14, 2023*, 2023.

[8] C. Smith, Y. Karayiannidis, L. Nalpantidis, X. Gratal, P. Qi, D. V. Dimarogonas, and D. Kragic, "Dual arm manipulation—a survey," *Robotics and Autonomous Systems*, vol. 60, no. 10, pp. 1340–1353, 2012.

[9] D. Surdilovic, Y. Yakut, T.-M. Nguyen, X. B. Pham, A. Vick, and R. Martin-Martin, "Compliance control with dual-arm humanoid robots: Design, planning and programming," in *2010 10th IEEE-RAS International Conference on Humanoid Robots (Humanoids)*, 2010, pp. 275–281.

[10] O. Khatib, "A unified approach for motion and force control of robot manipulators: The operational space formulation," *IEEE Journal on Robotics and Automation*, vol. 3, no. 1, pp. 43–53, 1987.

[11] Y. Nakamura, H. Hanafusa, and T. Yoshikawa, "Task-priority based redundancy control of robot manipulators," *The International Journal of Robotics Research*, vol. 6, no. 2, pp. 3–15, 1987.

[12] D. Ortenzi, R. Muthusamy, A. Freddi, A. Monteriù, and V. Kyrki, "Dual-arm cooperative manipulation under joint limit constraints," *Robotics and Autonomous Systems*, vol. 99, pp. 110–120, 2018.

[13] J. Lee, P. H. Chang, and R. S. Jamisola, "Relative impedance control for dual-arm robots performing asymmetric bimanual tasks," *IEEE Transactions on Industrial Electronics*, vol. 61, no. 7, pp. 3786–3796, 2014.

[14] S. Feng, E. Whitman, X. Xinjilefu, and C. G. Atkeson, "Optimization based full body control for the atlas robot," in *2014 IEEE-RAS International Conference on Humanoid Robots (Humanoids)*, 2014, pp. 120–127.

[15] F. Kanehiro, M. Morisawa, W. Suleiman, K. Kaneko, and E. Yoshida, "Integrating geometric constraints into reactive leg motion generation," in *2010 IEEE/RSJ International Conference on Intelligent Robots and Systems (IROS)*, 2010, pp. 4069–4076.

[16] J. Vaillant, A. Kheddar, H. Audren, F. Keith, S. Brossette, A. Escande, K. Bouyarmane, K. Kaneko, M. Morisawa, P. Gergondet *et al.*, "Multi-contact vertical ladder climbing with an hrp-2 humanoid," *Autonomous Robots*, vol. 40, no. 3, pp. 561–580, 2016.

[17] S. Tarbouriech, B. Navarro, P. Fraisse, A. Crosnier, A. Cherubini, and D. Sallé, "Dual-arm relative tasks performance using sparse kinematic control," in *2018 IEEE/RSJ International Conference on Intelligent Robots and Systems (IROS)*, 2018, pp. 6003–6009.

[18] B. Faverjon and P. Tournassoud, "A local based approach for path planning of manipulators with a high number of degrees of freedom," in *Proceedings. 1987 IEEE International Conference on Robotics and Automation*, vol. 4, 1987, pp. 1152–1159.

[19] D. Williams and O. Khatib, "The virtual linkage: a model for internal forces in multi-grasp manipulation," in *[1993] Proceedings IEEE International Conference on Robotics and Automation*, 1993, pp. 1025–1030 vol.1.

[20] Y. Zhang, J. Wang, and Y. Xu, "A dual neural network for bi-criteria kinematic control of redundant manipulators," *IEEE Transactions on Robotics and Automation*, vol. 18, no. 6, pp. 923–931, 2002.

[21] Y. Zhang, Z. Li, M. Yang, L. Ming, and J. Guo, "Jerk-level zhang neurodynamics equivalency of bound constraints, equation constraints, and objective indices for cyclic motion of robot-arm systems," *IEEE Transactions on Neural Networks and Learning Systems*, vol. 34, no. 6, pp. 3005–3018, 2023.

[22] G. Franklin, J. Powell, and M. Workman, *Digital Control of Dynamic Systems-Third Edition*, 11 2022.

[23] T. Yoshiike, M. Kuroda, R. Ujino, Y. Kanemoto, H. Kaneko, H. Higuchi, S. Komura, S. Iwasaki, M. Asatani, and T. Koshiishi, "The experimental humanoid robot e2-dr: A design for inspection and disaster response in industrial environments," *IEEE Robotics Automation Magazine*, vol. 26, no. 4, pp. 46–58, 2019.

[24] Y. Kanemoto, T. Yoshiike, M. Muromachi, and M. Osada, "Compact and high performance torque-controlled actuators and its implementation to disaster response robot," in *2018 IEEE International Conference on Robotics and Automation (ICRA)*, 2018, pp. 4057–4063.

[25] T. Hasegawa, H. Waita, T. Kawakami, Y. Takemura, T. Ishikawa, Y. Kimura, C. Tanaka, K. Sugiyama, and T. Yoshiike, "Powerful and dexterous multi-finger hand using dynamical pulley mechanism," in *2022 International Conference on Robotics and Automation (ICRA)*, 2022, pp. 707–713.

[26] "rviz - ROS Wiki," 2023. [Online]. Available: http://wiki.ros.org/rviz